SHAKING TABLE TEST AND NUMERICAL SIMULATION FOR SEISMIC SOIL-PILE-BRIDGE STRUCTURE INTERACTION IN LIQUEFIABLE GROUND

Liang Tang[1] Pengju Xu[2] Xianzhang Ling[3] Xia Gao[4]

[1] *Ph D Candidate, Department of Civil Engineering, Harbin Institute of Technology, Harbin, China*
[2] *Ph D Candidate, Department of Civil Engineering, Harbin Institute of Technology, Harbin, China*
[3] *Professor, Department of Civil Engineering, Harbin Institute of Technology, Harbin, China*
[4] *Ph.D Candidatet, Department of Civil Engineering, Harbin Institute of Technology, Harbin, China*
Email: hit_tl@163.com

ABSTRACT :
Here the investigation through shaking table test involving in the liquefaction characteristics of unfree ground and seismic response of single-pile-supported bridge structure is presented. The shaking table test, taking the destructive Shengli bridge in 1976 Tangshan earthquake as its prototype, was performed using the laminar shear box with depth of 2 m and plan dimensions of 2 m and 1.5 m, and the soil profile consisted of the lower level liquefiable saturated loose sand overlying non-liquefied silty clay crust. Galvanized iron wire and micro-concrete single-pile was used in the test. Bridge superstructure was modeled as the iron mass. The model was tested with a series of El Centro earthquake of varying level of shaking. The large-scale shaking table test involved intense shaking that lead to a significant degradation of strength and stiffness of soil due to liquefaction. Representative data that characterize important aspects of soil-pile interaction mechanics in liquefied ground were presented. The test results are analyzed and simulated in detail with FORTRAN program. This paper provides an insight into the numerical simulation of seismic soil-pile-structure interaction (SSPSI) in liquefiable ground studied in a shaking table facility. The numerical simulation of the complete soil-pile-bridge structure in liquefiable ground is conducted according to shaking test table using the finite element method. The matching of the experimental and numerical responses in the time domain is satisfying. Many important aspects of SSPSI in liquefiable ground that are apparent in the experiment are captured by the numerical simulation.

KEYWORDS:
Seismic soil-pile-structure interaction, Liquefiable ground, Numerical simulation, Shaking table test.

1. INTRODUCTION

One of the major sources of extensive damage to pile-supported bridges in the earthquakes is the occurrence of soil liquefaction, and the significance of liquefaction-related damage to piles had been clearly demonstrated under strong earthquake like the 1995 Hyogo–ken Nambu Earthquake, Japan (Kobe earthquake). In the 1976 Tangshan earthquake of China, many pile-supported structures had pile damages with the slight breakage of superstructures and the resulting bridges were destroyed, especially in liquefied ground. The soil liquefaction might reduce the inertia force of the superstructures, but the damage of the superstructure only resulting from the damage to piles was frequently observed. The seismic response of an engineering structure in liquefiable ground is greatly affected by the medium on which it is founded. Structural response is governed by the interplay between the characteristics of the soil, the structure and the input motion. Seismic soil-pile-structure interaction (SSPSI), as this phenomenon has become known, has been of research interest for the past 30 years. Compared with that on stiff ground, SSPSI in liquefiable ground had two more significant uncertainties on structural response related to the dynamic characteristics, the mechanism and the vibration energy which may be dissipated either by radiation waves, emanating from the vibrating foundation-structure system back into the soil, or by hysteretic material damping in the soil of SSPSI system in liquefiable soil. Laboratory based SSPSI studies involving in liquefiable ground generally employ a purpose designed soil container to hold the model. Shaking table models are generally much larger than centrifuge models. Thus, the space available for

instrumentation and actuators is greater and more subtle in loading, control and observation is feasible. Recently shaking table tests are causing great attention due to its effectiveness in dealing with the aseismatic questions of pile-supported bridge structures. Shaking table SSPSI studies in liquefiable ground and some valuable knowledge from shaking table tests have been reported by some scholars at home and abroad, especially from Japan and America. At present, there is a dearth of information regarding the numerical simulation of entire seismic soil-pile- bridge structure (SSPSI) systems in liquefiable ground subjected to the real earthquake motions feasible to the shaking table. Some facts indicate that the importance of considering seismic soil-pile-structure interaction in aseismic design of piles even in liquefied ground.

A series of shaking table tests under the successive support of National Natural foundation of China since 2002, were performed to understand the basic mechanisms of SSPSI in liquefiable ground, including the cases of single piles and pile groups, low cap pile groups and elevated cap pile groups, liquefiable ground and nonliquefiable ground, and different soil profile consisted of two horizontal soil layers with the upper layer of 0.3 m thick of normally consolidated silty clay and the lower layer of 1.6 m thick of the saturated sand and three horizontal soil layers with the upper layer of 0.3 m thick of normally consolidated silty clay, the middle layer of 1.2 m thick of the saturated sand and the lower layer of 0.4 m thick of soft clay, synoptically described in Figure 1. The aim of this paper is three-fold: (a) to provide details of a shaking table test (Test 4) featuring soil model included single-pile-supported bridge structure in liquefiable soil purposely designed to induce significant SSPSI in liquefiable soil, (b) to demonstrate that the response of the test model can be simulated accurately under the proper assumption despite the nonlinear liquefiable soil response associated with strong ground motion, and (c) to investigate both numerically and experimentally a few important features of SSPSI in liquefiable ground.

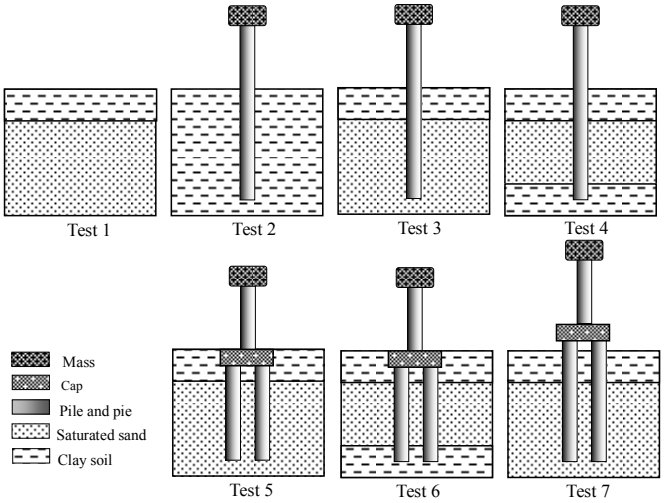

Figure 1 Sketch diagram of a series of shaking table tests achieved

2. TEST PROCEDURE

The details of the test including structure systems, soil profile and instrumentation are schematically illustrated in Figure 2. Shengli Bridges shown in Figure 3 was the prototype of the model test collapsed in 1976 Tangshan earthquake. Considering the capacity and the size of shaking table used at Tongji University, dimension scaling parameter was chosen as 1/10. A single-pile-supported bridge structure was used for the test. The superstructure mass was typically about 120 kg for the single pile. The single pile was the model of a prototype reinforced concrete pile 1 m in diameter, 25.2 m long. The model pile was prefabricated with fine-aggregate concrete and the galvanized iron wires, with diameter 0.1 m, length 2.52 m, and depth 1.7 m. Based on 8 tests, the concrete had an average 28-day compressive strength of 8.5 MPa. The soil profile used in the test consisted of two horizontal soil layers. The lower layer of 1.6m thick was medium-dense Shanghai sand with a non-uniformity coefficient of 3.0, mean particle diameter of 0.31 mm, specific gravity of 2.72, maximum void ratio of 0.961,

minimum void ratio of 0.570 and maximum diameter of 2 mm. The sand was prepared through the improved water pluviated method and then saturated. The coefficient of permeability of the saturated sand at relative density of 50% was typically 0.0045 cm/s. This above method for the desired saturated sand had been used in the previous 1-g model studies (e.g. Xianzhang Ling and Dongsheng Wang 2003). The upper layer of 0.3m thick was normally consolidated silty clay for the "model clay". The model clay had liquid and plastic limits of LL = 90% and PL =20%, and a plasticity index of PI= 85%. Also note that the water table was approximately at interface between the upper and lower soil layers.

Shaking table test was carried out using MTS shaking table facility at the State Key Laboratory for Disaster Reduction in Civil Engineering, Tongji University, Shanghai, China. The table can be input three-dimensional and six degree-of-freedom motions. The dimension of the table is 4m×4m, and the maximum payload is 25 000 kg. The shaking table can vibrate with two maximum horizontal direction accelerations of 1.2g and 0.8g, with a maximum acceleration of 0.7g vertically. The table has an operating frequency range of 0.1 to 50Hz and there are 96 channels available for data acquisition during testing progress.

A large-scale laminar shear box was designed by Lichu Fan et al (2000) and fabricated to study the mechanisms of seismic pile groups-soil-bridge structure interaction. The height of this shear box was 2 m and its plan dimensions were 2 m×1.5 m. In the test, the sponge cushion with 100 mm thickness was vertically set along the two inside walls perpendicular to the shaking direction for the purpose of decreasing the reflection of laminar box boundary on the seismic wave. In the shaking table test reported in this paper, acceleration response of the shear box was measured which was compared well with those of the soil layers at the same elevations.

The container was subjected to a series of El Centro earthquake events with varying level of shaking as representative ground motion input, listed in Table 1, beginning with very low-level shaking events to characterize the low-strain response of liquefiable soil and soil-structure systems. Successive events progressed through very strong motions with peak base accelerations of up to 0.5g. Every earthquake event was implemented after the pore pressure dissipation almost finished. The time scaled coefficient of scaled 0.15g El Centro earthquake was $1:\sqrt{10}$. To ensure an effective transmission of the table motion to the base of the test structure, the model base plate was firmly mounted on the shaking table through bolt connections.

Table 1 Earthquake Motions Used

Step	Earthquake event	Peak acceleration
Event 1	White noise（NS direction）	0.02g
Event 2	Scaled El Centro earthquake	0.15g
Event 3	El Centro earthquake	0.15g
Event 4	El Centro earthquake	0.5g

3. TEST RESULTS

3.1. White-noise excitation

The experimental system was firstly excited by the low-amplitude (0.02 g), broadband (0-50 Hz) white-noise to explore the frequency response of different components of the system. The natural frequency and the damping of the model systems were 10.5 Hz and 12.4%, respectively through the white noise input. The natural frequency of the empty container is about 1.2-1.4 Hz (10 to 12 Hz model) for the larger shaking events presented herein. There was huge difference of the natural vibration characteristics between the laminar box and the entire model systems, so the laminar box would not produce the negative effect on the dynamic properties of the model soil.

3.2. Liquefaction characteristics of ground

Test phenomena are shown in Figure 4. The following phenomena were summarized including: (1) waterspouts in ground surface didn't appear, the vibration amplitude of the ground surface and the pile were small, while the vibration frequency of the ground surface and the pile was relatively high under scaled 0.15g El Centro earthquake, (2) the top of sand layer was partly liquefied and the vibration amplitude of the pile top was still

rather small but the vibration frequency decreased to some degree under 0.15g El Centro earthquake, (3) under 0.5g El Centro earthquake, the whole sand layer was completely liquefied, sandboils and waterspouts occurred, the pile broke down at the depth of 14 cm above the upper soil interface, and the breakage range of the pile of 31cm long indicated that the build-in point of the pile in the soil always moved downward with the development of liquefaction. After the earthquake motion, lots of sandy hillocks formed by sandboils were distributed in the ground surface and the soil settlement ranged from 5cm to 8cm, especially the settlement of the local position was about 15 cm to 18 cm.

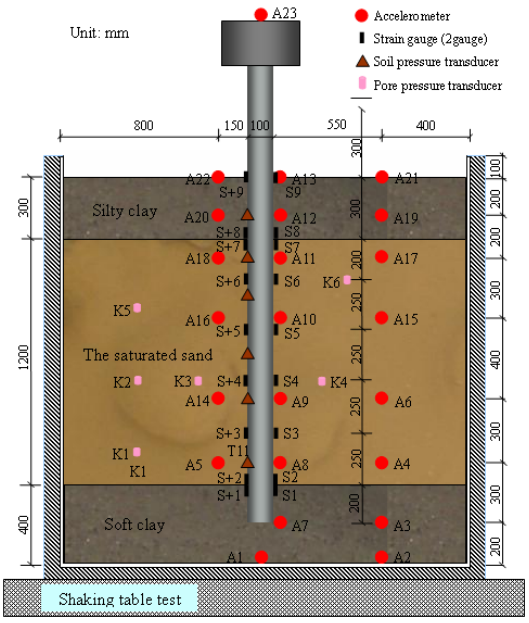

Figure 2 Shaking table test

Figure 3 The destructive Shengli Bridge

Figure 4 Macro-phenomena

The pore pressure peak ratios in sand along the depth are shown in Figure 5. The pore pressure peak changed a little, the pore pressure peak ratio notably increased from bottom to top and the pore pressure ratio in the middle and upper sandy layer were greater than 0.3, which agreed with slight soil liquefaction in the middle and upper sand layer, under scaled 0.15g El Centro earthquake and 0.15g El Centro earthquake. The pore pressure peak decreased in total from bottom to top mainly due to the easy drainage of the pore water in the upper part and the pore pressure peak ratio from bottom to top varied irregularly but was equal to or greater than 1, which indicated that the whole sand layer completely liquefied under 0.5g El Centro earthquake. The pore pressure of the sand instantaneously increased to larger value and didn't have an accumulative process under three earthquake events, and it's concluded that the accumulation of the pore pressure occurred near the time when the input earthquake motion reached the peak. The relationship of the occurrence time of the pore pressure peak with the depth is depicted in Figure 6. The dashed line in Figure 5 obtained from magnifying $\sqrt{10}$ times of the occurrence time of the pore pressure peak under scaled 0.15g El Centro earthquake nearly kept consistent with that under 0.15g El Centro earthquake. The occurrence time of the pore pressure peak lagged behind that of the acceleration peak of the ground under three earthquake events. The delay behavior of the pore pressure peak was more notable only

in the upper sand layer under scaled 0.15g El Centro earthquake and 0.15g El Centro earthquake, however it was more remarkable in the lower sand layer under 0.5g El Centro earthquake which was probably due to the accumulation and the difficult drainage of the pore water in the lower sand layer.

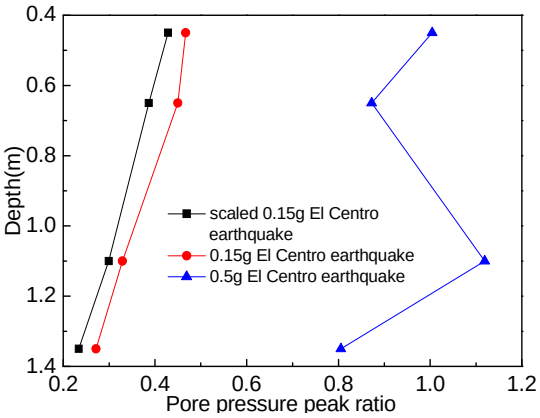

Figure 5 Relationship of pore pressure peak ratio and the depth

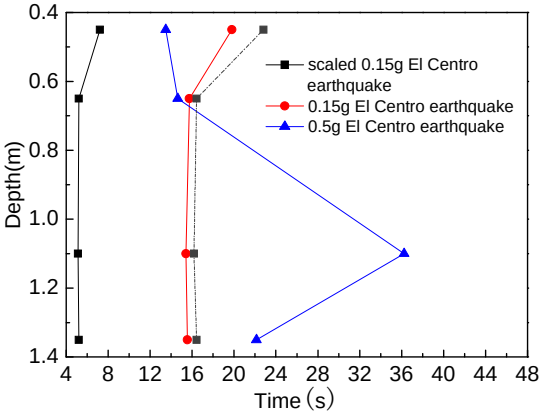

Figure 6 Relationship of the occurrence time of pore pressure peak with the depth

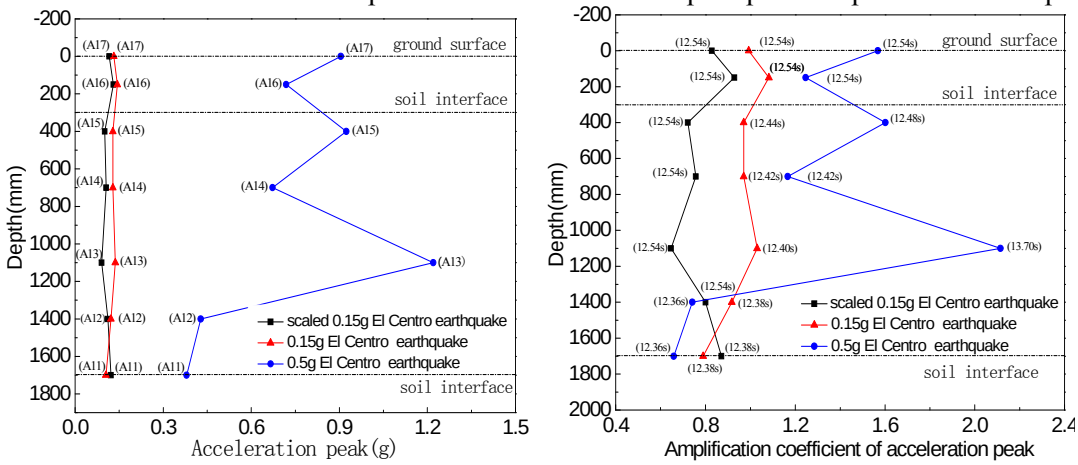

Figure 7 Acceleration peak and its amplification coefficient of ground versus the depth

Figure 7 shows the relationships of both the acceleration peak of the ground and its amplification coefficient defined as the acceleration peak divided by the input earthquake motion peak versus the depth. The acceleration peak of the ground almost remained uniform under scaled 0.15g El Centro earthquake and 0.15g El Centro earthquake; however the acceleration peak of the ground under 0.15g El Centro earthquake were greater than that under scaled 0.15g El Centro earthquake; the greater acceleration amplification coefficient more than 1 under 0.15g El Centro earthquake explained that the ground had a more intense dynamic response on 0.15g El Centro earthquake and a obvious damping action on scaled 0.15g El Centro earthquake which was in agreement with the macro-phenomena.

The acceleration peak of ground and its amplification coefficient presented the “increase-decrease” fluctuant change from bottom to top under 0.5g El Centro earthquake. That is mainly beacause that the fully liquefied sand exhibited the intense shear and flow behavior which caused the false phenomena of the significant amplification effect of the upper clay and the middle sand layer on 0.5g El Centro earthquake. The acceleration peak resulted from the strong shear flow of the liquefied sandy layer with the accelerometers, in other words, the amplification effect of the soil was induced by the shear and flow of liquefied sand but not the real ground amplification.

3.3. Behavior of pile

The acceleration peak and its amplification coefficient of the pile along the depth are shown in Figure 8. The accelerations peak of the pile with its amplification coefficient less than 1 almost kept invariable and the

acceleration peak of the pile top with the amplification coefficient greater than 1.5 responded remarkably, which implied that seismic response of the pile was restricted by the ground, and the approximately identical acceleration peak of the pile tip and its amplification coefficient indicated that the lower clay layer strongly and effectively restricted the pile under scaled 0.15g El Centro earthquake and 0.15g El Centro earthquake. The acceleration peak and its amplification coefficient of the pile in the upper clay layer and the sand layer under 0.15g El Centro earthquake were greater than those under scaled 0.15g El Centro earthquake, showing that the pile had a more evident dynamic response on 0.15g El Centro earthquake and was in agreement with the larger vibration amplitude of the pile in the test under 0.15g El Centro earthquake. The acceleration peak and its amplification coefficient of the pile tip were very large, and the acceleration peak and its amplification coefficient of the pile in the sand and the upper clay layer decreased from bottom to top, which was caused by the inertial force of the superstructure, and the fully liquefied sand resulting in the build-in point of the pile in the soil moved downward and the instantaneous slippage between the pile and soil which lead to the acceleration of the pile tip large under 0.5g El Centro earthquake. The acceleration peak and its amplification coefficient of the pile top were relatively great, which was caused by the breakage of the pile in liquefiable ground under 0.5g El Centro earthquake.

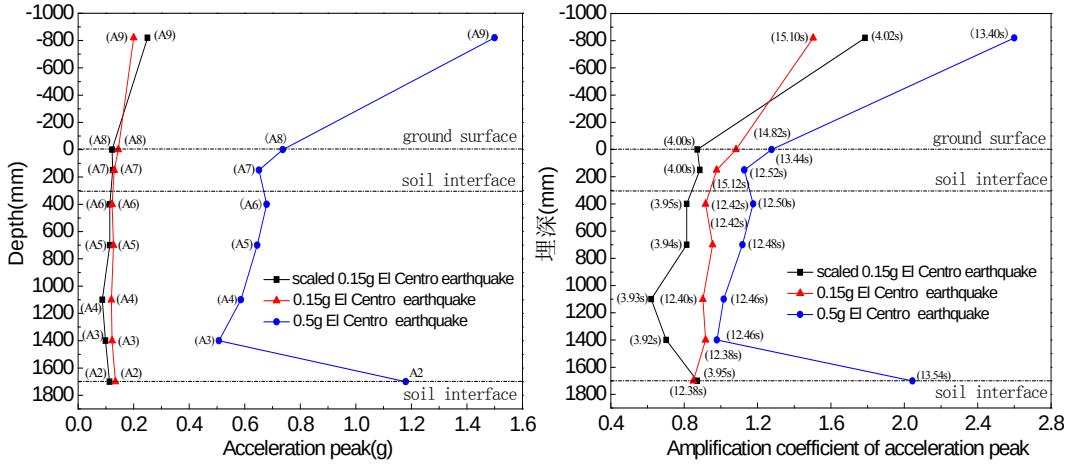

Figure 8 Acceleration peak and its amplification coefficient of the pile versus the depth

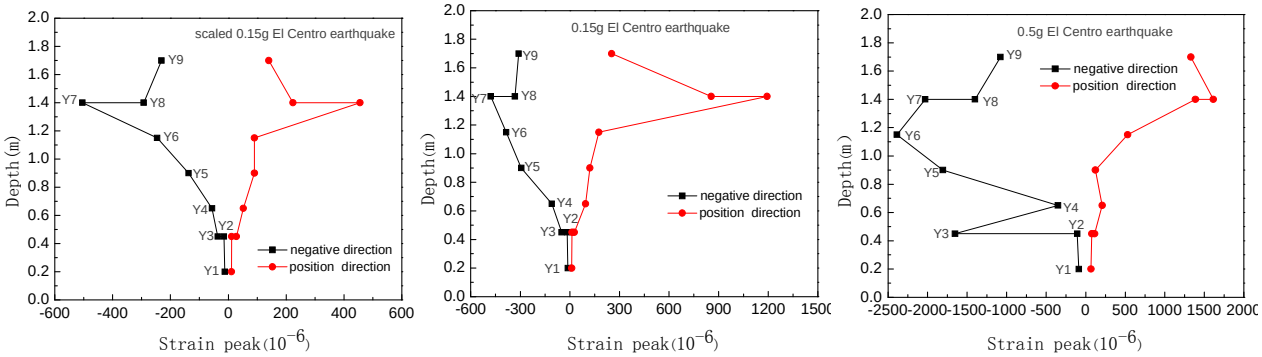

Figure 9 The strain peak on two sides of pile versus the depth

The relationship between the strain peak and the depth is illustrated in Figure 9. The strain peak of the pile increased in the sand and decreased in the upper clay layer from bottom to top, which was in agreement with the fact that the pile suffered from the damage more easily in the sand ground than in the clay ground, and the strain peak on two sides of the pile almost kept identical in value but opposite in direction under scaled 0.15g El Centro earthquake and 0.15g El Centro earthquake. The strain peak of the pile under 0.15g El Centro earthquake are much greater than that under scaled 0.15g El Centro earthquake due to the long duration of earthquake motion and the restriction of the lower clay layer resulted in the unconspicuous difference on the strain peak of the pile near the upper soil interface. Only under 0.15g El Centro earthquake did the strain peak on two sides of the pile in the upper soil interface have the poor symmetry due to the partial liquefaction of the sand. Under 0.5g

El Centro earthquake, the strain peak on two sides of the pile in the upper soil interface lost the symmetry, and the sudden change of the strain peak on the pile occurred in the upper and lower soil interface, especially in the lower soil interface; the strain peak of the pile in the soil was much greater than that of the pile above the ground surface due to the restriction of the upper clay layer and the inertial force of the superstructure and the appearance of the larger strain peak on the pile in the upper clay layer lead to the fracture of the pile, which displayed that the breakage of the pile during the earthquake was closely related to the initial force of superstructure. The maximum strain on the pile occurred in the upper soil interface under scaled 0.15g El Centro earthquake and 0.15g El Centro earthquake. The maximum strain along the pile occurred in the sand near the upper soil interface under 0.5g El Centro earthquake. The strain peak of the pile tip almost was zero due to the unfixed pile tip under three earthquake events.

4. NUMERICAL SIMULATION

Numerical model developed for the analysis of SSPSI in liquefiable ground was based on finite element method and took into account the progressive build up of the pore pressure due to earthquake loading without the pore pressure dissipation within the soil due to vertical drainage.

4.1. Basic assumptions

Basic assumptions for numerical simulation are as follows: (a) the upper clay layer, the middle liquefiable sand layer, the underlying clay layer and the base are horizontal, homogeneous and isotropic strata, the bedrock is supposed to be impervious with the motion of all the points being uniform and the water level is placed at the upper soil interface; (b) seismic wave is vertically propagating from bedrock, and the horizontal shear wave dominates the propagation; (c) the initial groundwater level is considered as drainage boundary; (d) There is non-drainage behavior of liquefiable soil during earthquake; (e) The assumption of plain strain is adopted in the method.

4.2. Constitutive relationship

The nonlinear, strain dependent and hysteretic behavior for Shanghai clay and sand soil are modeled using the modified hyperbolic stress-strain model (Pyker, 1979) based on Masing criterion as

$$\tau = \tau_0 + G_{\max}\left(\gamma - \gamma_0\right)\left[\frac{1}{1+\frac{\left|\gamma-\gamma_0\right|}{n\gamma_y}}\right] \qquad (4\text{-}1)$$

where, $G_{\max}$ is the initial maximum dynamic shear modulus, τ and γ are the dynamic shear stress and shear strain, respectively, τ_c and γ_c are the dynamic shear stress and strain at the turning point, τ_y is the dynamic shear strength, $\gamma_y = \tau_y / G_{\max}$ is reference dynamic strain, and $n = \left|\pm 1 - \tau_c / \tau_y\right|$ （1 for the upper semi-cycle of hysteretic curve and -1 for the lower semi-cycle） is loading factor. $G_{\max}$ and τ_y are given as

$$G_{\max} = A_1(\bar{\sigma}_0)^{C_3} \qquad (4\text{-}2)$$

$$\tau_y = A_2(\bar{\sigma}_0)^{B_3} \qquad (4\text{-}3)$$

where $\bar{\sigma}_0$ is the average normal pressure, C_3 and B_3 are the factors. Especially, the dynamic shear module and the shear strength of test sand are amended through the following method.

4.3. Parameters modification

Dynamic shear modulus $G_{\max}$ and shear strength τ_y are modified with varying pore pressure during earthquake loading. $G_{\max}$ and τ_y are modified through the empirical formula in each stress cycle due to pore pressure increment given as

$$G_{\max,N} = G_{\max,N-1} g\left(\frac{\bar{\sigma}_{0,N}}{\bar{\sigma}_{0,N-1}}\right)^{C_3} \tag{4-4}$$

$$\tau_{y,N} = \tau_{y,N-1} g\left(\frac{\bar{\sigma}_{0,N}}{\bar{\sigma}_{0,N-1}}\right)^{B_3} \tag{4-5}$$

where subscript N-1 and N respectively relate to the corresponding parameters before and after modification. Hyperbolic stress-strain model is used to evaluate equivalent damping ratio and just is given as

$$\beta = \beta_{\max}\left(1 - G/G_{\max}\right) = \left(28 - 1.5\lg N\right)\left(1 - G/G_{\max}\right) \tag{4-6}$$

where $\beta_{\max}$ is the maximal damping ratio of stress cycle, G is the secant modulus and N is the number of stress cycle.

In seismic response analysis of post-liquefiable ground, the pore pressure ratio is 0.99 when it is beyond 0.99 or the dynamic shear strain reaches 0.0002, and the dynamic shear modulus of liquefied soil(G_{liq}) is defined as $G_{liq} = 0.0125 G_{\max}$ by experience.

4.4. Model of pore pressure generation

The pore pressure generation is calculated through the empirical pore pressure model developed by Ishibashi and Sherif (1977), given as

$$\Delta U_N^* = \left(1 - U_{N-1}^*\right)\bar{N}\left(\frac{\tau_N}{\bar{\sigma}_{N-1}}\right)^a \tag{4-7}$$

$$\bar{N} = \frac{A_1 \cdot N}{N^{A_2} - A_3} \tag{4-8}$$

The relations between $\Delta U_N^* / \left(1 - U_{N-1}^*\right)$ and $\tau_N / \bar{\sigma}_{N-1}$ and between cyclic effect factor $\bar{n}$ and cyclic number N obtained from the liquefaction tests are respectively given as

$$\frac{\Delta U_N^*}{1 - U_{N-1}^*} = \bar{n}\left(\frac{\tau_N}{\bar{\sigma}_{N-1}}\right)^{A_4} \tag{4-9}$$

where $\tau_N / \bar{\sigma}_{N-1}$ is the stress ratio, $\Delta U_N^* = \Delta U_N / \bar{\sigma}_0$ is the ratio of pore pressure increment to the initial average effective stress in the Nth cycle, U_{N-1}^* is the ratio of pore pressure to the initial average effective stress in the (N-1)th cycle, $\bar{\sigma}_{N-1}$ is the average effective stress in the (N-1)th stress cycle, τ_N is the stress amplitude in the Nth cycle, $\bar{n}$ is the cyclic effect factor, and C_1, C_2 and A_4 are test parameters.

In that case the ground motion is divided into the parcels of different magnitudes and the equivalent number of cycle is calculated for each parcel separately. In the model, the pore pressure increment is calculated at the end of loading or reloading.

4.6. Modeling and Simulation for shaking table test

The FE model is composed of three parts: soil, pile and Goodman element. Figure 11 shows the mesh of the proposed numerical model for the test, where Number 1 to 14 is element number for the pile, Number 1 to 18 is Goodman element number, and Number 1 to 101 is element number for the soil. In this analysis, therefore, the arbitrary convex quadrilateral element model is used for the horizontal soil including liquefied sand and clay. The single pile is simulated in elasticity state and subdivided into the four-node beam element. Meanwhile, based on the master-slave surface displacement relation and Timoshenko beam theory, the influence coefficient of shear deformation ϕ determined using the equation $\phi = 12EI / GA_s l^2$ was introduced into beam element

stiffness matrix to account for the size effect of the pile, where A_s is the effective shear resistant area,

$A_s = kA$, $k = \dfrac{Q^2}{A\int_A \tau_\alpha^2 dA}$, $\tau_\alpha = \dfrac{3}{2}\dfrac{Q}{A}\dfrac{(h/2)^2 - y^2}{(h/2)^2}$,

h is the pile diameter, l is the beam length, A is the section area, y is the distance from interesting point to section center, E is the elastic modulus, Q is the shearing force, and I is the rotational inertia. The pile above the ground surface is simplified to connected with the centralized mass as the upper bridge structure by using the connection bending stiffness $K_u = 12EJ/l^3$, where E, J and l are the elastic modulus, the cross section rotary inertia and the length of the pile, respectively. Pile and soil interface is treated as the Goodman element. In the analysis, both sides of the vertical boundary walls, the nodes are fixed in the vertical direction and the soil-box interface in the test is represented by parallel spring and damper boundary including viscous damper with the viscosity coefficient $C_b = \rho c$ and linear spring with the elastic coefficient $K_b = G/2r_b$ are applied to the truncating boundary, where r_b is the radius of truncation radius. In addition, foundation bottom is considered as the fixed boundary in the horizontal direction. The nodal coordinates at the base are fixed both in the vertical direction and are free in the horizontal direction. Besides, the slip at the interface between the liquefied layer and clay layer is negligible. Pile is modeled as isotropic elastic beam elements and single-pile-supported superstructure is considered as SDOF structure. The dynamic equation for SSPSI systems are established and given as

$$\begin{bmatrix} M_u & 0 \\ 0 & M_s \end{bmatrix}\begin{Bmatrix} \ddot{r}_u \\ \ddot{r}_s \end{Bmatrix} + \begin{bmatrix} C_u & 0 \\ 0 & C_s \end{bmatrix}\begin{Bmatrix} \dot{r}_u \\ \dot{r}_s \end{Bmatrix} + \begin{bmatrix} k_u & 0 \\ 0 & k_s \end{bmatrix}\begin{Bmatrix} r_u \\ r_s \end{Bmatrix} = -\begin{Bmatrix} E_{u,x}\ddot{u}_{g,x} \\ E_{s,x}\ddot{u}_{g,x} + E_{s,y}\ddot{u}_{g,y} \end{Bmatrix} \tag{4-10}$$

where, M_u is the mass matrix of superstructure (1×1), M_s is the mass matrix of substructure, C_u is the horizontal damping matrix of connection of bridge structural mass and single pile, C_s is the damping matrix of substructure, K_u is the bending stiffness matrix of pile, K_s is the stiffness matrix of substructure, r_u is the horizontal displacement vector of superstructure（1×1）, r_s is the horizontal and vertical displacement vector of substructure, $E_{u,x}$ is the indicating column matrix for mass matrix of superstructure, $E_{s,x}$ is the indicating column matrix for mass matrix of substructure in the x-direction（the mass of each node in the y-direction of the corresponding position in the column vector is 0）, $E_{s,y}$ is the indicating column matrix for mass matrix of substructure in the y direction（the mass of each node in the x-direction of the corresponding position in the column vector is 0）, $\ddot{u}_{g,x}$ is the input ground motion acceleration in the x-direction, and $\ddot{u}_{g,y}$ is the input ground motion acceleration in the y-direction. The element stiffness matrix of soil is set up through isoparametric element analysis. The Rayleigh damping is adopted and the dynamic equations are solved using the Wilson-θ integration method.

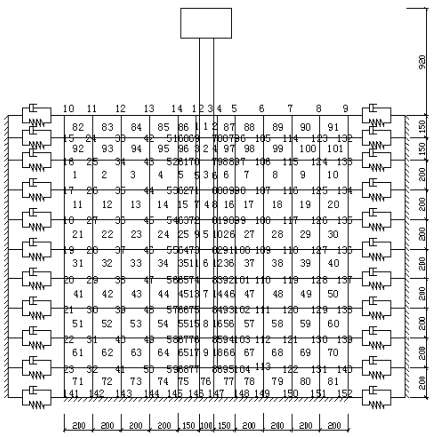

Figure 12 The finite element model mesh for the test

5. SIMULATED RESPONSE

Dynamic finite element program for the mentioned method designed by FORTRAN90 can be used to demonstrate and analyze SSPSI in liquefiable ground. The seismic input motions in the analysis are chosen from the measured input earthquake motion record.

The comparative results between the acceleration results of the pile under three earthquake events obtained from the selected accelerator A8 in the test and those of the corresponding node with its number as 85 in the analysis model are displayed in Figure 12. The comparison indicates that the acceleration peak from the test and the numerical analysis gradually increases under three different earthquake events and the time to reach acceleration peak is consistent with the time when the input earthquake motion reaches the peak; however the difference seems to be more obvious under 0.5g El Centro earthquake than under other earthquake event. Besides, the experimental and simulated acceleration of the pile recorded within the soil under three earthquake events increases gradually first and finally becomes smaller and smaller from bottom to top. Compared with that under 0.15g El Centro earthquake, the acceleration amplitude and the peak magnification coefficient of the pile decrease a little under scaled 0.15g El Centro earthquake, which indicates that the damage of engineering structures during the earthquake with the same intensity is closely dependent on shaking duration. As a whole, the trend of the simulated acceleration of the pile is accordance with that from the test, nevertheless the calculated results sometimes are smaller than the test results, especially under 0.5g El Centro earthquake. That is mainly because the pile responds in elastic state, the pore pressure in sand is relative small and the effect of the local liquefied ground on the pile has not been functioned yet under scaled 0.15g El Centro earthquake and 0.15g El Centro earthquake. Moreover, the growth and dissipation of the pore pressure in the test coexist under 0.5g El Centro earthquake, while in the analysis the pore pressure increment is calculated during every stress cycle, the dissipation is neglected and the effect of liquefiable ground on seismic response of the pile is underestimated.

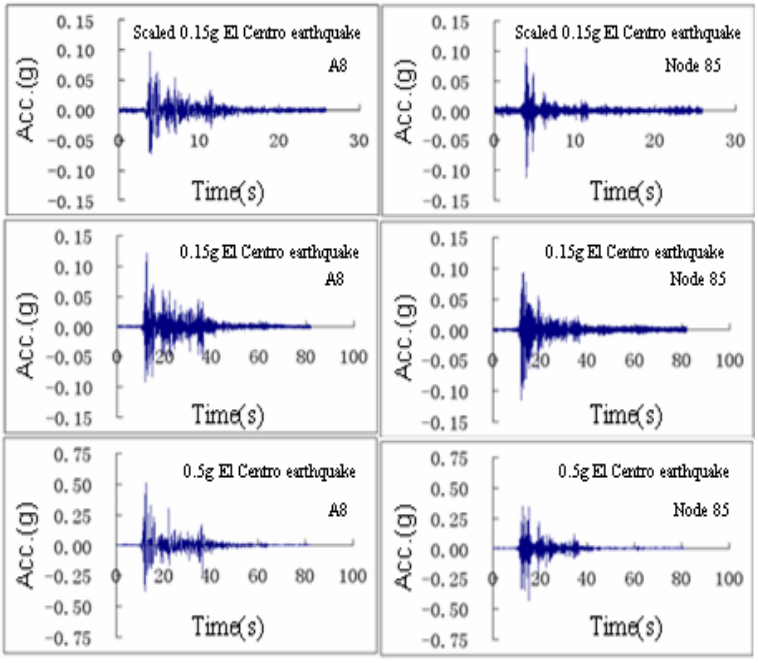

Figure 12 Acceleration time histories of the pile under three El Centro earthquake events

Figure 13 presents the comparison between the experimental strain record of the pile measured by S1 and the simulated strain of the corresponding node in the FEM. The agreement between the strain time histories , no matter for the peak value, the time to reach the peak, or for the change trend, is very good at all sensor locations. In the test and numerical simulation, the strain peak increases gradually, the time to reach strain peak is almost the same as the time to reach input earthquake motion peak; the minimum strain value of pile for the test and the analysis appears in the lower clay layer, while the maximum strain value appears in the upper clay layer near the

upper soil interface, which is against the cognition that the maximum strain value should occur in the sand layer. Meanwhile, the experimental and simulated strain peak of the pile increases first and then decreases gradually under three earthquake events. Similarly, the difference of the dynamic strain between the test and the analysis is also more remarkable under 0.5g El Centro earthquake.

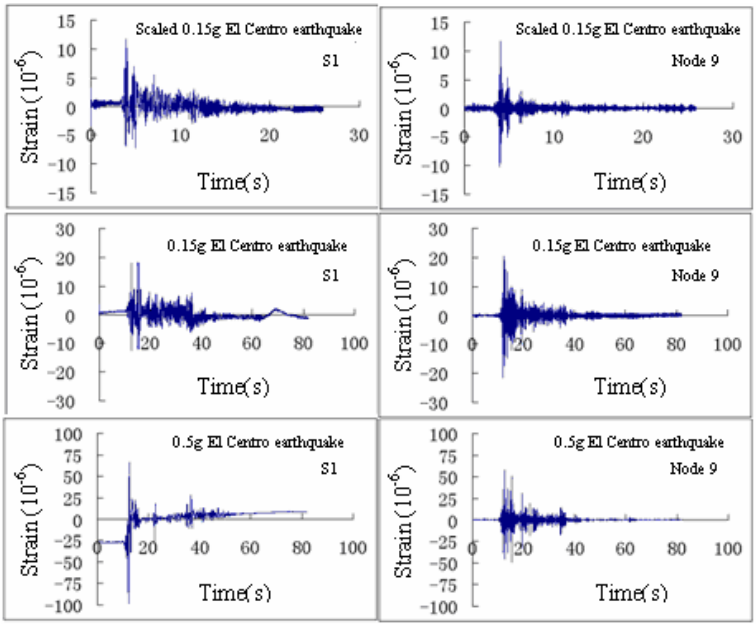

Figure 13 Strain time histories of pile under three El Centro earthquake events

6. CONCLUSION

A shaking table test of soil-single pile-structure system designed to induce significant SSPSI in liquefiable ground was conducted at State Key Laboratory for Disaster Reduction in Civil Engineering of Tongji University, China. The shaking table test well reproduced the main macro-phenomena of the soil liquefaction and the structure damage induced by earthquake. Data sets generated by subjecting the laboratory model to real earthquake motions were compared to numerical simulations of the system conducted in the nonlinear behavior, even though liquefied soil is expected under strong ground shaking.

Under scaled 0.15g El Centro earthquake and 0.15g El Centro earthquake, the acceleration peak of ground almost kept invariable from bottom to top; the pore pressure quickly attained the maximum after the input earthquake motion reaching its peak，and then dissipated quickly，in addition，there was little difference of the pore pressure peak of the sand between near the pile and far away from the pile. The pile had the elastic dynamic deformation and the strain peak increased from bottom to top, the strain peak of the pile in the sand were much greater and the strain peak of the pile in the upper clay layer were much greater than that of the pile above the ground surface under scaled 0.15g El Centro earthquake and 0.15g El Centro earthquake. The pore pressure quickly increased and slowly attained the peak with the slow dissipation velocity meanwhile the pore pressure peak of the sand near the pile were much greater than that of the sand far away from the pile; the acceleration peak of the pile was more intense, the cracking of the upper pile occurred in the clay layer and the pile was broken down in the upper clay near the soil interface under 0.5g El Centro earthquake. It could be concluded that the effect of the distance away from the pile on the pore pressure mainly depended on the intensity of the input earthquake motion.

ACKNOWLEDGMENTS

This work is part of a project on “large-scale shaking table tests for seismic pile-soil-bridge structure interaction in liquefiable ground” funded by National Natural foundation of China and shaking table tests have been carried out at State Key Laboratory for Disaster Reduction in Civil Engineering of Tongji University, China. This

support is gratefully acknowledged.

REFERENCE

Abdoun, T and Dobry, R. (2002). Evaluation of pile foundation response to lateral spreading. Soil Dynamics and Earthquake Engineering **22:3**, 1051-1058.
Boulanger, R. W., Curras, C. J., Kutter, B. L., et al. (1999). Seismic soil-pile-structure interaction experiments and analyses. Journal of Geotechnical and Geoenvironmental Engineering, ASCE **125:9**, 750-759.
Finn, W.D.L and Fujita, N. (2002). Piles in liquefiable soils: seismic analysis and design issues. Soil Dynamics and Earthquake Engineering **22**, 731-742.
Feng Wanling and Shi Zhaoji. (1988). Analysis for pore water pressure increment of saturated standard sand under deviatoric stress consolidation. Earthquake Resistant Engineering **12:4**, 67-73.
Ganve, T., Yamazaki, F., Ishizak, H., et al. (1998). Response Analysis of the Higashi-Kobe bridge and surrounding soil in the 1995 Hyogokennanbu Earthquake. Earthquake Engineering and Structural Dynamics **27:3**, 557-576.
Hardin, B., Iwasaki, T., Tatsuoka, F., et al. (1978). Shear moduli of sands under cyclic torisional shear loading. Soil and Foundations **18:1**, 39-56.
Hardin, B. and O. Drnevish. (1972). Shear modulus and damping in soils: design equation and curve. Journal of the Soil Mechanics and Foundations Division **98:7**, 667-692.
Ishibashi, I., and Zhang, X.. (1993). Unified dynamic shear moduli and damping ratios of sand and clay. Soils and Foundations **33:1**, 182-191.
Kawashima, K. and Unjoh, S.. Impact of Hanshin-Awajie Earthquake on seismic design and seismic Strengthening of highway bridges. Earthquake Engineering and Structural Dynamics**13:2**, 211-240.
Ling Xianzhang, Guo Mingzhu, Wang Dongsheng et al. (2006). Large-scale shaking table model test of seism response of bridge of pile foundation in ground of liquefaction. Rock and Soil Mechanics **27:1**, 7-10. (in Chinese)
Ling Xianzhang, Wang Chen and Wang Cheng. (2004). Scale modeling method of shaking table test of dynamic interaction of pile-soil-bridge structure in ground of soil liquefaction. Chinese Journal of Rock Mechanics and Engineering **23:3**, 450-456. (in Chinese)
Ling Xianzhang, Wang Dongsheng et al. (2002). Large-scale shaking table model test of dynamic soil-pile-bridge structure interaction in ground of liquefaction. China Civil Engineering Journal, 2002, **22:4**, 51-59. (in Chinese)
Ling Xianzhang, Wang Lixia, Wang Dongsheng et al. (2005). Study on large-scale shaking table proportional model test of the dynamic property of foundation in unfree ground of liquefaction. China Journal of Highway and Transport **18:2**, 34-39. (in Chinese)
Liu Jingbo and Wang Zhenyu. (2002). 3D Finite element analysis of large dynamic machine foundation considering soil-structure interaction[J]. Engineering Mechanics **19:3**, 34-38.
Pyke R. (1979). Nonlinear Soil Models for Irregular Cyclic Loadings. Journal of Geotechnical Engineering Division **105:6**, 715-726.
Shi Zhaoji and Wang Lanmin. (1999). Dynamic property of soil: liquefaction potential and evaluation of liquefaction harmfulness, Seismic press, Beijing. (in Chinese)
Wu Xiaoping , Sun Limin , Hu Shide et al. (2002). Development of laminar shear box used in shaking table test. . Journal of Tongji University **30:7**, 781-785. (in Chinese)